Journal of ELECTRONIC MATERIALS, Vol. 43, No. 5, 2014
DOI: 10.1007/s11664-014-3096-3

Improved Calculation of the Electronic and Optical Properties of Tetragonal Barium Titanate

ASHFAQUL ANWAR SIRAJI[1,2] and M. SHAH ALAM[1,2,3]

1.—Department of Electrical and Electronic Engineering, Bangladesh University of Engineering and Technology (BUET), Dhaka 1000, Bangladesh. 2.—Department of Electrical and Electronic Engineering, Northern University, Dhaka, Bangladesh. 3.—e-mail: shalam@eee.buet.ac.bd

The electronic and optical properties of tetragonal barium titanate ($BaTiO_3$) have been investigated by use of first-principles density functional theory on a plane wave basis, by use of norm-conserving pseudopotentials in the localized density approximation. For accuracy, experimental lattice parameters reported in the literature were used. The band structure, total and partial density of states (DOS), and Born effective charges of tetragonal $BaTiO_3$ were obtained from first-principles calculations. The partial DOS and Born effective charges indicate that the Ti–O bonds are partially covalent and the Ba–O bonds are partially ionic. The complex dielectric functions for ordinary and extraordinary optical polarization were calculated, and were in reasonable agreement with those from previous first-principles calculations. The refractive index, extinction coefficient, reflectivity, and energy-loss spectrum for both types pf polarization were calculated from the complex dielectric function; the results obtained were an improvement on other published results.

Key words: Barium titanate, density functional theory, optical properties, ABINIT

INTRODUCTION

Density functional theory (DFT) has been successfully used for ground-state theoretical calculations for crystalline solids.[1] Although calculation of excited states by use of DFT is not rigorously justified, interpretation of Kohn–Sham (KS) states on the basis of excited states has been successful for a variety of materials.[2] As a result, DFT has been successfully used to study the optical response of crystalline solids.[3] $BaTiO_3$, a ferroelectric material, has been of great interest to industry because its bandgap is in the visible range. The optical properties of $BaTiO_3$ have been measured experimentally. Cai et al.[4] measured the optical properties of a $BaTiO_3$ thin film grown by the sol–gel technique. Wada et al.[5] measured the dielectric properties of $BaTiO_3$ fine particles by using the infrared reflection method in the THz range.

(Received July 21, 2013; accepted February 24, 2014; published online March 13, 2014)

In addition to experimental measurement, there have been several theoretical first-principles calculations of the optical properties of $BaTiO_3$. Samantaray et al. investigated the optical properties of cubic barium strontium titanate alloy ($Ba_xSr_{1-x}TiO_3$) by use of the localized density approximation (LDA), as implemented in CASTEP software.[6,7]. Cai et al.[8] investigated the optical properties of cubic $BaTiO_3$ by using the full potential, linear, augmented plane wave method with the generalized gradient approximation (GGA). Ahuja et al.[9] calculated the complex dielectric function and refractive index of tetragonal $BaTiO_3$ by using the full potential (self consistent) linear muffin tin orbital method. Sanna et al. calculated the electronic band structure and the complex dielectric function of the cubic and tetragonal phases of $BaTiO_3$ by using the projected augmented wave method (PAW) with GGA within DFT.[10]. Wang et al.[11] calculated the elastic, polarization, and electrostrictive properties of $BaTiO_3$ in several phases by using the projected augmented wave method with the LDA within DFT. Wahl et al.[12]

calculated the structural, electronic, and phonon properties of tetragonal and cubic $BaTiO_3$ by use of the projected augmented wave method with several types of exchange correlation functional within DFT.

One of the most important properties of tetragonal $BaTiO_3$ (with *the P4mm* space group) is its noncentrosymmetry. This particular structure ensures that the crystal is uniaxially anisotropic. However, first-principles analysis of the detailed anisotropic optical properties of tetragonal $BaTiO_3$ has not yet been conducted. In this work, the optical properties of $BaTiO_3$ for ordinary and extraordinary polarization were calculated by use of the LDA on a plane wave basis without using the muffin tin approximation. To reinforce the results, the detailed density of states (DOS) and KS band structure were also calculated.

COMPUTATIONAL DETAILS

The first-principles calculations of the electronic and optical properties were performed within DFT on a plane wave basis and using norm-conserving pseudopotentials. The exchange correlation energy in the LDA was computed by using the Teter rational polynomial parametrization fit to Ceperley–Alder data without considering the spin polarization.[13] The core of the atoms was represented by the pseudopotentials of the respective atoms. The O $2s^2 2p^4$, Ba $5s^2 5p^6 6s^2$ and Ti $3s^2 3p^6 4s^2 3d^2$ electrons were explicitly treated as valence electrons. It was found that a plane wave basis cutoff of 20 Ha gave a sufficiently converged result for the optical properties. To calculate the electronic properties a cutoff energy of 35 Ha was assumed. Integrations over the Brillouin zone were performed by summing over a sampled $18 \times 18 \times 20$ *k-point* grid generated by the Monkhorst–Pack scheme[14]. This sampling was enough to achieve self consistent solution where the tolerance on maximum difference of energy was 1×10^{-12} Ha. During the non-self consistent part of the calculations, the tolerance on the residual of squared wave-function was 1×10^{-20}. The calculated bandgap for $BaTiO_3$ was 1.744 eV whereas the experimental value is 3.2 eV. This demonstrates the well known problem of underestimation of the bandgap inherent in LDA methods. To match the experimental bandgap, a scissor shift of 1.434 eV was used.

The tetragonal phase of $BaTiO_3$ has the space group *P4mm*. Shirane et al.[15] determined the lattice constants of tetragonal $BaTiO_3$ experimentally; they were $a = 3.986$ Å and $c = 4.026$ Å. We used these lattice constants in our calculations. The crystal structure has a Ba atom at the origin, a Ti atom at the body center, and O atoms at the face centers. The Ti and O atoms are slightly displaced, which is the origin of anisotropy of the crystal. The optical properties of $BaTiO_3$ can be found from the frequency-dependent complex dielectric function:

$$\epsilon(\omega) = \epsilon_1(\omega) + i\epsilon_2(\omega), \tag{1}$$

where ϵ_1 is the real part and ϵ_2 is the imaginary part. The complex dielectric function is found from the equation:[16]

$$\epsilon_{ij}(\omega) = \delta_{ij}(\omega) + \frac{4\pi}{\Omega}\sum_{nmk} f_{nm}(k)\frac{\mathbf{r}^i_{nm}(\mathbf{k})\mathbf{r}^j_{mn}(\mathbf{k})}{\omega_{nm}(\mathbf{k}) - \omega}, \tag{2}$$

where ϵ_{ij} is the ijth component of the dielectric tensor and $r_{nm}(k)$ are the wavevector ($\mathbf{k}$)-dependent complex position matrix elements. To evaluate Eq. (2), the position matrix is necessary. Gonze and co-authors[17,18] established an equivalence between the off-diagonal matrix elements of the position matrix and the off-diagonal matrix elements of the derivative of the wave function with respect to the wave vectors in three directions. Hence, calculation of the derivative with respect to the wave vectors was sufficient to calculate the position matrix. The ABINIT[17,19–23] package was used to calculate the ground-state wave function and its derivative with respect to the wave vectors. The formulae used to calculate refractive index $n(\omega)$, extinction coefficient $k(\omega)$, reflectivity $R(\omega)$, and energy loss spectrum $L(\omega)$ of $BaTiO_3$ were:[6]

$$n(\omega) = \frac{1}{\sqrt{2}}\left[\sqrt{\epsilon_1(\omega)^2 + \epsilon_2(\omega)^2} + \epsilon_1(\omega)\right]^{\frac{1}{2}}, \tag{3}$$

$$k(\omega) = \frac{1}{\sqrt{2}}\left[\sqrt{\epsilon_1(\omega)^2 + \epsilon_2(\omega)^2} - \epsilon_1(\omega)\right]^{\frac{1}{2}}, \tag{4}$$

$$R(\omega) = \frac{(1 - n(\omega)^2) + k(\omega)^2}{(1 + n(\omega)^2) + k(\omega)^2}, \tag{5}$$

and

$$L(\omega) = \frac{\epsilon_2(\omega)}{\epsilon_1(\omega)^2 + \epsilon_2(\omega)^2}. \tag{6}$$

RESULTS

Electronic Structure

The band structure of tetragonal $BaTiO_3$ along the high-symmetry points is shown in Fig. 1. The figure shows that the bandgap is indirect.

The maximum of the valence band occurs at the point, whereas the minimum value of conduction band occurs at the M point. As stated previously, the calculated bandgap is 1.744 eV, which is close to previously calculated values.[8,10] The experimental value of the optical bandgap is 3.2 eV, however.[24] This discrepancy is because of the established underestimation of conduction band energies by

DFT.[25] To make the results realistic, a scissor shift of 1.434 eV was used in subsequent calculations.

The total and partial DOS (pDOS) are shown in Fig. 2.

The pDOS are calculated per atom. In the range −30 eV to 10 eV, there are four valence bands and one conduction band. As expected, the peaks in the total DOS and the pDOS correspond to each other.

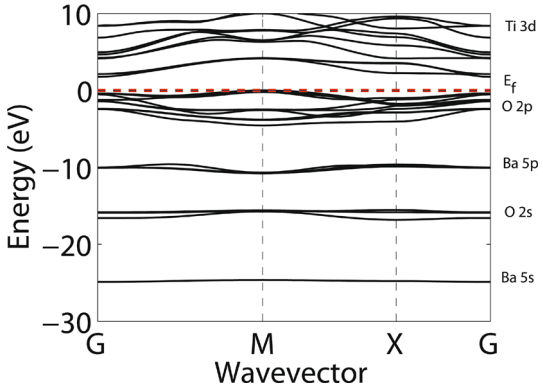

Fig. 1. The energy band structure of $BaTiO_3$ along the high symmetry points $-M-X-$. The dominant contributor in a band is indicated by the text on the right vertical axis.

Peak A is caused by the peak in the pDOS of Ba-5s. Peak B corresponds to the peak in the pDOS of O-2s. Peak C is because of the peak in the pDOS of Ba-5p. Peak D corresponds to the peak in the pDOS of O-2p. Peak E is because of the peak in the pDOS of Ti-3d.

Examining the total DOS and its decomposition by use of the pDOS, it is possible to associate each band in the band structure with different states of the atoms, as shown in Fig. 1. The bands above E_f mainly result from Ti-3d states and 0-2p states and constitute the conduction band (CB).

The pDOS gives further insight into the electronic structure. Sizable overlap of the DOS of Ti-3d and O-2p is apparent from Fig. 2b, c; this suggests that electrons are shared between these two states. Ideally, the Ti–O bond should be an ionic bond. Sharing between Ti-3d and O-2p leads to a partially covalent bond, however. This nature of Ti–O bond is elucidated from the Born effective charges of the five atoms in the unit cell. The Born effective charges were calculated from derivatives of ground-state wave functions with respect to the electric field associated with atomic displacement.[19] The Born effective charges of the atoms of tetragonal $BaTiO_3$, with the nominal charges, which are the ionic charges of the atoms, are shown in Table I. The

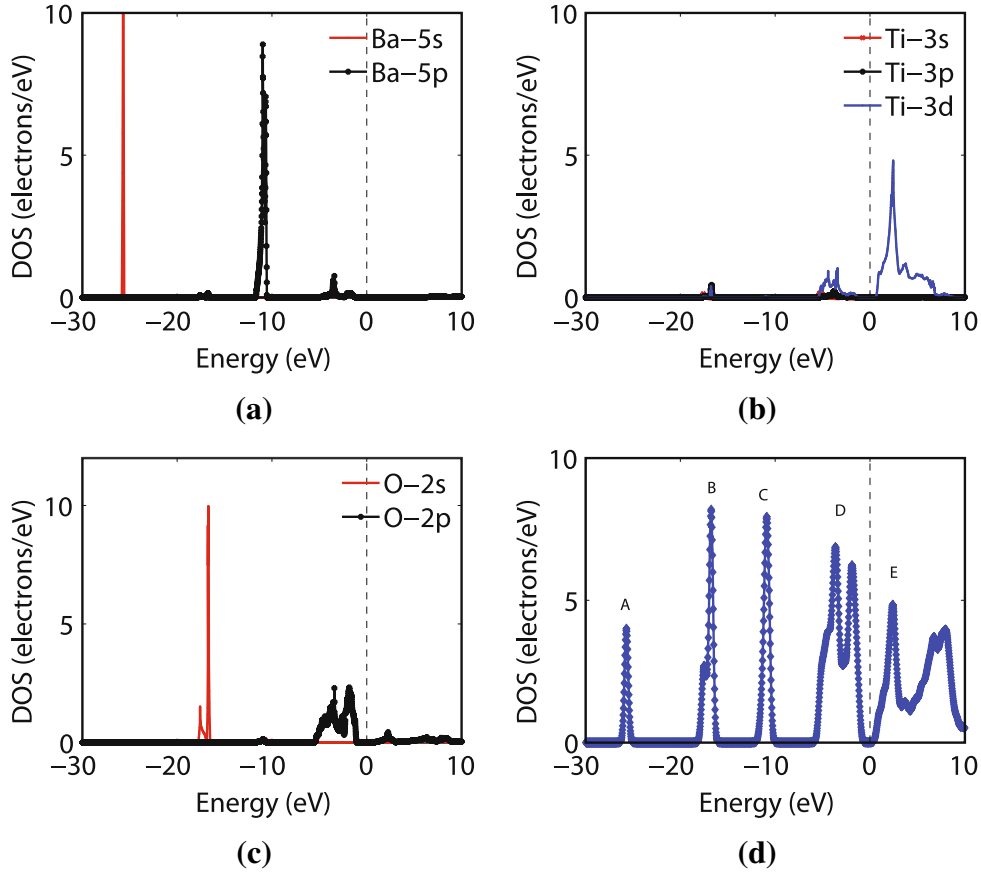

Fig. 2. (a) pDOS of Ba, (b) pDOS of Ti, (c) pDOS of O, and (d) total DOS of the atoms in $BaTiO_3$. Each peak is marked with a letter.

Table I. Born effective charge tensors of the atoms in tetragonal $BaTiO_3$

Atom	Nominal charge	Born effective charge (Z)		
Ba	2	2.720	0.000	0.000
		0.000	2.720	0.000
		0.000	0.000	2.818
Ti	4	7.033	0.000	0.000
		0.000	7.033	0.000
		0.000	0.000	5.687
O1	−2	−2.018	0.000	0.000
		0.000	−2.018	0.000
		0.000	0.000	−4.636
O2	−2	−2.128	0.000	0.000
		0.000	−5.626	0.000
		0.000	0.000	−1.944
O3	−2	−5.626	0.000	0.000
		0.000	−2.129	0.000
		0.000	0.000	−1.943

values in the table are in agreement with those reported in Ref. 26.

From Table I it is apparent that the effective charges of the Ti and O atoms deviate significantly from their nominal ionic values. This clearly indicates that the nature of the Ti–O is not fully ionic but rather ionic-covalent instead. This observation is in agreement with previous works.[27]

Optical Properties

$BaTiO_3$ is an anisotropic material. It's optical properties are dependent on the polarization of the incident light. We considered the cases when the incident light is polarized along the axis of spontaneous polarization of the crystal © axis) and when the incident light is polarized in the plane perpendicular to the c axis. The first case corresponds to the extraordinary polarization and the second case to the ordinary polarization. The calculated real and imaginary parts of the complex dielectric functions for both cases are shown in Fig. 3. For comparison, the results obtained by Cai et al.[8], Ahuja et al.[9], and Bauerle et al.[28] are also included.

Bauerle et al. determined the optical properties of $BaTiO_3$ by observing the near-normal incidence reflectance spectra experimentally. It should be noted that Cai et al. calculated the optical properties of the cubic phase of $BaTiO_3$ and Bauerle et al. determined the optical properties of single-crystal $BaTiO_3$ with no anisotropy. Although we used the tetragonal phase of $BaTiO_3$ for our calculations, the value $c/a = 1.025$ indicates that the anisotropy is very small and, thus, the comparisons are valid.

From Fig. 3a and b, it can be seen that all the structures in the experimental data of Bauerle et al. are reproduced in our result, as intended. The positions of the local minima M_1, M_2 and M_3 in $\epsilon_1(\omega)$

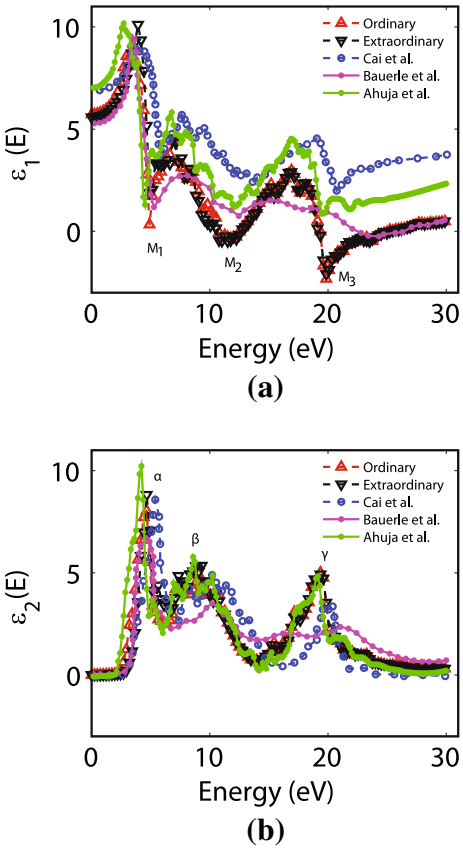

Fig. 3. (a) Real and (b) imaginary parts of the calculated complex dielectric function for the ordinary and extraordinary polarization plotted against photon energy.

and the local maxima α, β and γ in $\epsilon_2(\omega)$ of our results and those of Cai et al., Ahuja et al., and Bauerle et al. are shown in Table II. From the table it is apparent our calculation predicts the extreme points of the experimental data of Bauerle et al. more accurately at lower energy. However, the intensity of the peaks and the depths of the troughs in our results are different from the experimental data and our results become less accurate at higher energy. This deviation between the experimental results and our results is because we considered a limited number of bands and ignored excitons in our calculations. There are, also, some unwanted ripples in our results; these can be eliminated by denser sampling of the irreducible Brillouin zone (IBZ) and use of a greater number of plane waves. We could not perform our calculations with denser sampling and a greater number of plane waves because of hardware limitations. Our calculation predicts the positions of the extreme points in $\epsilon_1(\omega)$ and $\epsilon_2(\omega)$ with greater accuracy than the methods of Cai et al. and Ahuja et al. Cai et al. also overestimates the intensities of the peaks. Our results are not a good match with those of Cai et al. because, first, the bandgap and lattice constants in our calculation are closer to the experimental values, and, second, we used a denser mesh for sampling the IBZ

Table II. The positions (eV) of the troughs in $\epsilon_1(\omega)$ and the peaks in $\epsilon_2(\omega)$ from Fig. 3

	M_1	M_2	M_3	α	β	γ
This work	3.192	4.906	19.850	4.661	9.314	19.360
Cai et al.[4,8]	4.060	5.837	20.790	5.387	10.19	20.390
Bauerle et al.[28]	3.342	5.282	20.790	4.595	10.22	21.040
Ahuja et al.[9]	2.714	4.523	19.450	4.221	8.593	19.150

Table III. Average absolute deviation of the results of Cai et al., Ahuja et al., and of our work from the experimental results of Bauerle et al.

	Cai et al.	Ahuja et al.	Our calculation
$\epsilon_1(\omega)$	2.543	1.599	0.775
$\epsilon_2(\omega)$	1.035	1.097	0.796

compared with the $12 \times 12 \times 12$ grid used by Cai et al. Conversely, Our results are similar to those from Ahuja et al., because, similarly to our calculations, Ahuja et al. used an LDA approximation with the scissor approximation, and the crystal structure used in their calculations was close to that used in our calculations.

Taking the experimental results of Bauerle et al. as reference, we calculated the average absolute differences between the $\epsilon_1(\omega)$ and $\epsilon_2(\omega)$ of Cai et al., Ahuja et al., and our calculation. The average absolute differences were calculated by taking the sum of the absolute differences between ϵ_1 and ϵ_2 of Bauerle et al. and those of the other cases for all corresponding photon energies; we then calculated the mean for all the photon energies. The results are summarized in Table III. From the table it is apparent our results are more accurate than those from Cai et al. and Ahuja et al. The reason for this improved accuracy is that we used experimentally obtained lattice constants in our calculations and matched the experimental bandgap by using an appropriate scissor shift.

From Figs. 1 and 2, it was found that the peak α originates from the interaction between the O-2p and Ti-3d states, the peak β originates from the interaction between the O-2p and higher-energy conduction bands, whereas the peak γ is largely because of interactions between Ti-3d, O-2s, and Ba-5p. The most dominant peak is because of the interaction between the Ti-3d and O-2p bands.

The refractive index and the extinction coefficient were calculated from ϵ_1 and ϵ_2 by use of Eqs. (3) and (4). The results are shown in Fig. 4, in which the results from this work are compared with those reported by Cai et al., Ahuja et al., and Bauerle et al.

In Fig. 4a, the results from Cai et al. and Ahuja et al. and our results are in reasonable agreement, but all of these deviate from the experimental

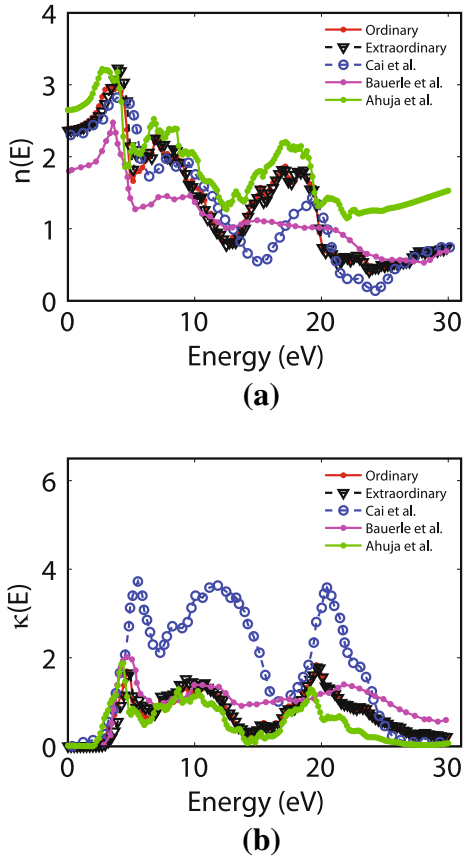

Fig. 4. Calculated refractive index (a) and extinction coefficient of $BaTiO_3$ for ordinary and extraordinary polarization (b) plotted against photon energy.

results of Bauerle et al. Among the theoretical calculations, however, our results match the experimental data most closely. Similarly, in Fig. 4b our results are in better agreement with the experimental results than those of Cai et al. and Ahuja et al. It is apparent from Fig. 4a that $n(\omega)$ in the two directions are not equal. The difference between $n(\omega)$ for the two types of polarization is shown in the Fig. 5, with results reported by Wemple et al.[29] and Ahuja et al. δn is known as the birefringence magnitude.

From Fig. 5, it is apparent that the magnitude of the birefringence of tetragonal $BaTiO_3$ increases slowly for incident photon energy within the optical range ($E < 4$ eV). The experimental results of Wemple et al. are indicative of overestimation of the

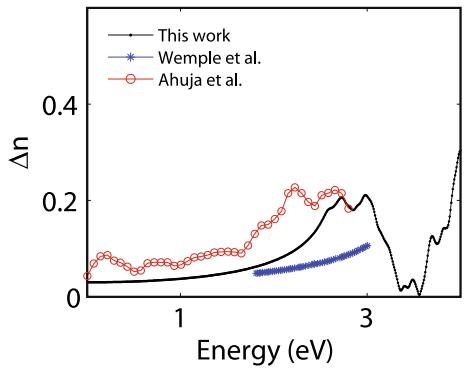

Fig. 5. Difference between $n(\omega)$ for ordinary and extraordinary polarization.

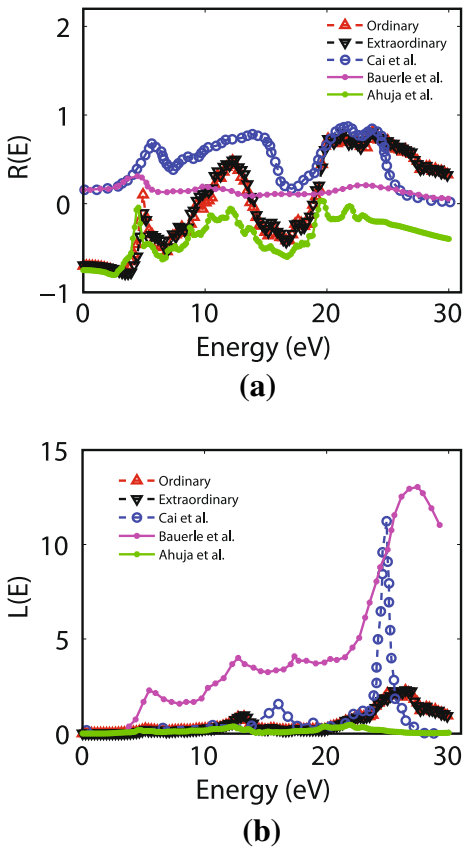

Fig. 6. Calculated reflectivity (a) and energy loss spectrum (b) of $BaTiO_3$, for ordinary and extraordinary polarization, plotted against photon energy.

birefringence by our method of calculation; our results are more accurate than those of Ahuja et al., however. In our calculation, we assumed there are no antiparallel domains. The crystals used by Wemple et al. contained random antiparallel domains, however, which reduced anisotropy; this explains the overestimation by our method. Because Ahuja et al. used a similar arrangement of ordinary and extraordinary axes, their method also overestimates the experimental results. Our method of calculation was more accurate (as explained), hence our results are closer to the experimental results. Similar to the refractive index, the extinction coefficient is also different for ordinary and extraordinary polarization. The maximum extinction coefficients for ordinary and extraordinary polarization were found to be 1.835 and 1.783, respectively.

The reflectivity and energy-loss spectrum were calculated from ϵ_1 and ϵ_2 by use of Eqs. (6) and (5). The calculated results and those obtained by Cai et al., Ahuja et al., and Bauerle et al. are shown in Fig. 6.

In Fig. 6a, the results of Cai et al. consistently overestimate the experimental results of Bauerle et al.; the results of Ahuja et al. consistently underestimate the experimental results. In our work the reflectivity was calculated by use of the same method as used by Ahuja et al. but our result is closer to the experimental result. The reflectivity spectrum $R(\omega)$ contains several peaks starting from 4.9 eV, as seen in Fig. 6a. This first peak corresponds to the first local maximum of $\epsilon_2(\omega)$ at 4.6 eV, as shown in Fig. 3b. It is apparent from Fig. 6b that none of the theoretically calculated loss spectra is a very good match with the experimental loss spectrum. This is because only a limited number of loss mechanisms can be taken into account in DFT calculations. However, the loss spectra calculated in our work matches those obtained by use of other first-principles calculations.

CONCLUSION

The electronic and optical properties of tetragonal $BaTiO_3$ for ordinary and extraordinary polarization have been investigated by use of DFT with the LDA as implemented in the ABINIT package. Experimentally obtained values of lattice constants and bandgaps were used for better accuracy. The total and partial DOS per atom were also calculated. The pDOS and Born effective charges of the individual atoms indicate that The Ti–O bond was partially covalent whereas the Ba–O bonds were largely ionic, in agreement with previously reported results. The valence bands of the crystal were found to consist of O-2s states and the conduction bands were Ti-3d and O-2p in nature. The complex dielectric function was calculated for a large range of photon energy. The peaks on the imaginary part of the dielectric part were traced back to the interaction between the Ti-3d states and the O-2s, O-2p, and Ba-5p states. The least intense peak results from the interaction between the Ti-3d and O-2p states. The optical properties of tetragonal $BaTiO_3$ in both the ordinary and extraordinary directions were calculated. The frequency-dependent refractive index, extinction coefficient, reflectivity, and energy-loss spectrum were also calculated. The frequency-dependent birefringence of $BaTiO_3$ was

calculated and compared with experimental results. The calculated results were in good agreement with experimental results and were more accurate than previously published results from DFT calculations. For optoelectronic and photonic applications in which dispersion data are necessary, our method of calculation can be a reasonable substitute for expensive experiments.

REFERENCES

1. O. Diéguez, K.M. Rabe, and D. Vanderbilt, *Phys. Rev.* **72**, 144101 (2005).
2. C. Ambrosch-Draxl and J.O. Sofo, *Comput. Phys. Commun.* **175**, 1 (2006).
3. M. Tang, D. He, and L. He, *Physica B* **406**, 3154 (2011).
4. W. Cai, C. Fu, J. Gao, Q. Guo, X. Deng, and C. Zhang, *Phys. B* **406**, 3583 (2011).
5. S. Wada, H. Yasuno, T. Hoshina, H. Kakemoto, Y. Kameshima, T. Tsurumi, and T. Shimada, *J. Eur. Ceram. Soc.* **26**, 1807 (2006).
6. C. Samantaray, H. Sim, and H. Hwang, *Physica B* **351**, 158 (2004).
7. CASTEP, Castep Developers Group (CDG), United Kingdom. http://www.castep.org.
8. M.Q. Cai, Z. Yin, and M.S. Zhang, *App. Phys. Lett.* **83**, 2805 (2003).
9. R. Ahuja, O. Eriksson, and B. Johansson, *J. Appl. Phys.* **90**, 1854 (2001).
10. S. Sanna, C. Thierfelder, S. Wippermann, T.P. Sinha, and W.G. Schmidt, *Phys. Rev.* **83**, 054112 (2011).
11. J.J. Wang, F.Y. Meng, X.Q. Ma, M.X. Xu, and L.Q. Chen, *J. Appl. Phys.* **108**, 034107 (2010).
12. R. Wahl, D. Vogtenhuber, and G. Kresse, *Phys. Rev.* **78**, 104116 (2008).
13. S. Goedecker, M. Teter, and J. Hutter, *Phys. Rev.* **54**, 1703 (1996).
14. H.J. Monkhorst, and J.D. Pack, *Phys. Rev.* **13**, 5188 (1976).
15. G. Shirane, H. Danner, and R. Pepinsky, *Phys. Rev.* **105**, 856 (1957).
16. S. Sharma and C. Ambrosch-Draxl, *Phys. Scr.* **2004**, 128 (2004).
17. X. Gonze, *Phys. Rev.* **55**, 10337 (1997).
18. R.W. Nunes and X. Gonze, *Phys. Rev.* **63**, 155107 (2001).
19. X. Gonze and C. Lee, *Phys. Rev.* **55**, 10355 (1997).
20. X. Gonze, B. Amadon, P.M. Anglade, J.M. Beuken, F. Bottin, P. Boulanger, F. Bruneval, D. Caliste, R. Caracas, M. Ct, T. Deutsch, L. Genovese, P. Ghosez, M. Giantomassi, S. Goedecker, D. Hamann, P. Hermet, F. Jollet, G. Jomard, S. Leroux, M. Mancini, S. Mazevet, M. Oliveira, G. Onida, Y. Pouillon, T. Rangel, G.M. Rignanese, D. Sangalli, R. Shaltaf, M. Torrent, M. Verstraete, G. Zerah, and J. Zwanziger, *Comput. Phys. Commun.* **180**, 2582 (2009).
21. X. Gonze, G. Rignanese, M. Verstraete, J. Betiken, Y. Pouillon, R. Caracas, F. Jollet, M. Torrent, G. Zerah, and M. Mikami et al., *Z. Kristallogr.* **220**, 558 (2005).
22. S. Sharma, J.K. Dewhurst, and C. Ambrosch-Draxl, *Phys. Rev.* **67**, 165332 (2003).
23. ABINIT, The ABINIT Group, Open source collaborative project. http://www.abinit.org.
24. K. Suzuki, and K. Kijima, Jpn. *J. Appl. Phys.* **44**, 2081 (2005).
25. D.S. Sholl and J.A. Steckel, *Density Functional Theory: A Practical Introduction* (Wiley, New York, 2009).
26. W. Zhong, R.D. King-Smith, and D. Vanderbilt, *Phys. Rev. Lett.* **72**, 3618 (1994).
27. P. Ghosez, J.P. Michenaud, and X. Gonze, *Phys. Rev.* **58**, 6224 (1998).
28. D. Bauerle, W. Braun, V. Saile, G. Sprssel, and E. Koch, *Z. Phys. B* **29**, 179 (1978).
29. S.H. Wemple, M. Didomenico Jr, and I. Camlibel, *J. Phys. Chem. Solids* **229**, 1797 (1968).